Journal of Food Engineering 373 (2024) 112019

Contents lists available at ScienceDirect

Journal of Food Engineering

journal homepage: www.elsevier.com/locate/jfoodeng

Influence of material characteristics on plant-based milk alternative properties

K. Kramm [a,*], A. Roucher [b], J. Busom Descarrega [b], M. Ambühl [b], J. Kammerhofer [c], V. Meunier [b], S. Heinrich [a]

[a] Hamburg University of Technology, Institute of Solids Process Engineering and Particle Technology, Denickestraße 15, 21073, Hamburg, Germany
[b] Nestlé Research, Vers-Chez-Les-Blanc, Route du Jorat, 1005, Lausanne, Switzerland
[c] Nestlé Product Technology Center, Nestléstraße 3, 3510, Konolfingen, Switzerland

ARTICLE INFO

Keywords:
Plant protein
Fiber
Food powder
Emulsion
Spray drying
Homogenization

ABSTRACT

Plant-based milk alternatives are gaining increasing relevance in the food industry, but the influence of plant proteins and fibers on the specific product properties has not yet been explored. In this study, the influence of soy protein isolate and the oat fiber β-glucan on the emulsion and powder properties of plant milk alternatives is analyzed. The components exhibit different behavior at the oil-water interface after homogenization, thereby affecting droplet size distribution, dynamic viscosity and emulsion stability in terms of electrostatic repulsion. To determine the interactions of the components at the interface, the individual raw materials soy protein isolate and oat bran as well as mixtures of both were investigated. The measurements highlight variations between the fiber component and the plant protein source at the interface. The identified differences in emulsion characteristics also manifest in spray drying with different particle sizes and lipid encapsulation efficiencies.

1. Introduction

Consumers are increasingly tending towards plant-based milk alternatives (PBMA) compared to conventional cow's milk (Statista, 2023). Thereby, the reasons are diverse and can be attributed, for example, to conditions such as lactose intolerance and milk allergy, lifestyle choices or the selection of a more sustainable food product (Aydar et al., 2020; Romulo, 2022; Yadav et al., 2017). PBMA are distinguished as a more environmentally friendly product as a result of lower CO_2 emissions and water consumption during production (Aydar et al., 2020; Romulo, 2022). This effect is also evident in the anticipated sales growth of plant-based milk products, significantly enhancing their industrial relevance (Aydar et al., 2020; Statista, 2023).

PBMA belong in the liquid form to oil in water (O/W)- emulsions, in which the dispersed oil phase is present as droplets in the continuous water phase. Emulsifying additives are used to stabilize the emulsion and facilitate the droplet breakup mechanism (Armbruster et al., 1991; Köhler, 2010). In the food industry, proteins often accumulate at the interface between oil and water phases and thus reduce the interfacial tension (Leal-Calderon et al., 2007). For the optimization of product properties such as stability and structure, the mechanical homogenization techniques of the rotor/stator system and high-pressure homogenization are applied (Kivelä et al., 2010). In Armbruster et al. (1991) and Yadav et al. (2017), reduced droplet size distributions of the disperse phase are described by the deforming forces acting during homogenization, exceeding the form-retaining interfacial forces and causing the breakup of aggregates and lipid droplets. To convert the liquid PBMA into a powdered form with an encapsulated dispersed oil phase embedded in an amorphous carbohydrate or protein matrix (Fuchs et al., 2006; Palzer et al., 2012), the O/W emulsions are dried using a spray dryer. The liquid product to be dried is first atomized with a nozzle, in which the solvent at the droplet surface has a higher partial pressure than the solvent in the drying gas. As a result of the partial pressure difference, the solvent water evaporates and the viscosity of the PBMA liquid droplet increases until a rubbery state is reached. Gianfrancesco et al. (2008) reported that this state is achieved at different moisture contents and surface temperatures depending on the emulsion composition. Moreover, amorphous substances in the liquid droplet can form a sticky surface, causing the particle to create porous agglomerate structures on contact with others (Palzer, 2007). The literature describes the

Abbreviations: DE, dextrose equivalent; EE, encapsulation efficiency; OB, oat bran; PBMA, plant-based milk alternative; SPI, soy protein isolate.

* Corresponding author.
E-mail address: kathrin.kramm@tuhh.de (K. Kramm).

https://doi.org/10.1016/j.jfoodeng.2024.112019
Received 7 November 2023; Received in revised form 8 February 2024; Accepted 19 February 2024
Available online 20 February 2024

stickiness temperature at 20–40 °C above the material-specific glass transition temperature at viscosities between 10^6 and 10^8 Pa • s (Bhandari, 2013; Gianfrancesco et al., 2008; Palzer, 2009).

In this study, a PBMA product with soy proteins as a protein source with a high nutritional value and oat bran to add fiber to the recipe was investigated. Both raw materials are characterized by positive health effects if consumed and functional properties that have a beneficial effect on the product (Aydar et al., 2020; Agbenorhevi et al., 2011; D'Adamo and Sahin, 2014; Kivelä et al., 2010; Zhang et al., 2009). However, the combination of soy proteins and oat fibers in PBMA and their influence on the emulsion and powder properties has not been researched to date. In particular, the integration of both components into a complex formulation for the manufacturing of the powdered food product is necessary to identify the influence of the applied technologies and process parameters on the material components and properties of the PBMA formulations. The results of this study can be used for the targeted regulation of PBMA product properties and thus enable optimization, for example with regard to reconstitution and storage stability.

2. Materials and methods

2.1. Materials

In the study, a plant-based alternative to conventional cow's milk was used. The considered simplified model system was intended to enable the transfer of the gained knowledge to more complex systems. The investigation was conducted with the raw materials glucose syrup with a dextrose equivalent (DE) of 21, soy protein isolate, sunflower oil and oat bran by integration into a formulation. In particular, the combination of the plant-based components soy protein isolate and oat bran in the complex composition with the carbohydrate and lipid source has not yet been published and thus provides fundamental insights for the optimization of PBMA products. The raw material Glucidex DE 21 (Azelis, Germany) was used for the amorphous polysaccharide glucose syrup DE 21. Soy protein isolate (SPI) from the product line VEGACON® 90S (Eurosoy, Germany) conduced as the protein source and was characterized by a crude protein content in dry matter according to DIN EN ISO 16634–1:2009 of 91.3% and an ash content of 4.55% with moisture content of the raw material of 5.8 g/100g. The lipid component was sunflower oil (Bressmer & Francke, Germany), which had a fatty acid content of palmitic acid C16:0 of 6.4%, stearic acid C18:0 of 3.5%, oleic acid C18:1 of 32.5% and linoleic acid C18:2 of 57.3%. The raw material oat bran (OB) (Mühle Schlingemann, Germany) was used to introduce the fiber β-glucan in the model system. OB was featured by a β-glucan content of 4.5 g/100g, fiber content of 11.4 g/100g, protein content of 138 g/kg and a Total Kjedahl Nitrogen of 22 g/kg.

Formulations were created from the components of the model system, enabling the influences of primarily protein and fiber on the formation of the PBMA product to be identified. Table 1 presents the plant powder (PP)- formulations as a function of the various components and set concentrations. In each composition, one component was used in a higher concentration compared to the other formulations. In composition PP1, the fiber content was more pronounced, while in PP2, SPI was incorporated at a higher concentration, and in PP3, glucose syrup DE 21 was utilized at a higher level. An equalization of the ingredients between the formulations is not possible, as the individual components are limited in the used concentration. The set concentration in the formulations is the maximum concentration at which processing and stability of the product can still be guaranteed. The composition PP3 represents the reference recipe in the study, as the raw material used to a greater extent has already been described in detail in the literature and PP3 is therefore intended to show the influence of the fiber component and the protein source in relation to the other formulations.

Table 1
Overview of the formulations PP1, PP2 and PP3 in regards to raw material composition.

Formulation	Glucose syrup DE 21 [$\%_{wt}$]	Soy protein isolate [$\%_{wt}$]	Sunflower oil [$\%_{wt}$]	Oat bran [$\%_{wt}$]
PP1	53	20	20	7
PP2	50	38	10	2
PP3	68	20	10	2

2.2. Production process of the plant-based alternative

2.2.1. Emulsion preparation

Prior to high-pressure homogenization, a crude emulsion was prepared. Therefore, the raw materials were added to the water phase and were pre-homogenized by the high-performance disperser T 50 Ultra Turrax (IKA, Germany) with an intensity of 6,000 rpm. Based on preliminary tests, the formulations PP1 and PP3 were produced with a solid content of 30% to demineralized water. Due to the significant increase in viscosity in PP2 as a result of the higher concentration of SPI, the solid content had to be reduced to 20%. Otherwise, the homogenization step with the high-pressure homogenizer would not have been possible and the influence of viscosity on the subsequent process steps and product properties would only allow a limited comparison between the PBMA formulations. The dispersed phase of the emulsion consists of the sunflower oil and the continuous phase contains the glucose syrup DE 21, SPI and OB. The plant proteins introduced by mainly the SPI and to a smaller extent from the OB act as emulsifiers in the system. The pre-homogenization step was followed by laboratory-scale high-pressure homogenization using the TwinPanda 600 (GEA, Germany). The two-stage lab homogenizer was operated in a single passage flow with pressures of 250/50, 350/100 and 450/150 bar. The temperature of the pre-homogenized emulsion before entering the high-pressure homogenizer was around 20 °C and based on the set pressures, the temperature increased after the pass to 27–36 °C. The emulsion was prepared in triplicates for each formulation. The measurement results shown are the mean value and standard deviation calculated from the trials.

2.2.2. Spray drying

The PBMA powders from the homogenized emulsions were produced using the laboratory spray dryer B-290 (Büchi, Switzerland). The spray dryer operated on the co-current principle and the emulsion was atomized by a two-fluid nozzle with external liquid mixing. The nozzle had a liquid insert with a diameter of 0.7 mm to a total cap diameter of 1.5 mm. A total emulsion volume of 700 mL, homogenized with 250/50 bar at one passage and constant temperature, was dried per formulation at a spray rate of 10 g/min, inlet temperature of 220 °C and outlet temperature between 74 and 120 °C. The aspirator was operated at 85% corresponding to a volume flow of 33 m^3/h and the spray gas flow rate was set at 40 mm on the rotameter, which was equivalent to a flow rate of 667 l/h. Powder production was conducted in duplicates for each formulation; the results are given as mean values with standard deviations.

2.3. Analysis of emulsion properties

2.3.1. Droplet size distribution

The droplet size distribution of the emulsion formulations was analyzed in at least triplicates using the wet dispersion unit of the Mastersizer 3000 (Malvern Panalytical, United Kingdom) (Guldiken et al., 2023). The occurrence of settling or separation of the sample in the water dispersant is effectively prevented by utilizing a stirrer operating at a speed of 1,600 rpm. The sample concentration was controlled by the obscuration parameter, which was kept within a range of 1–5%. The plant emulsions were measured with a refractive index of 1.6 and an absorption index of 0.001 in relation to the material system. For the calculation of the droplet size distribution, spherical droplets were

assumed and evaluated according to the Mie theory (Mie, 1908).

2.3.2. Zeta potential

To assess emulsions stability, zeta-potential measurements were performed with a Zetasizer Nano ZS (Malvern Panalytical, United Kingdom). The measurement method was based on Guldiken et al. (2023) and was further adapted. To avoid multiple scattering due to excessive sample concentration and consequent impairment of the measurement results, the emulsion sample was diluted 1:200 with demineralized water. The zeta potential was measured in triplicates with the cuvettes DTS1070 (Malvern Panalytical, United Kingdom) and analyzed in dependency of the pH value measured with inoLab pH 7110 (WTW, Germany).

2.3.3. Rheological investigation

The rheological properties of the emulsions were determined with the rheometer Kinexus Pro (Malvern Panalytical, United Kingdom) in order to explain the flow behavior in the process steps and the material properties in more detail. The investigation was conducted following Agbenorhevi et al. (2011) and Guldiken et al. (2023) with modifications. Rotation measurements were performed with the cone and plate geometry at 25 °C and a pre-tempering time of 10 min. Cone and plate geometry is characterized by uniform shear conditions in the gap, fast temperature adaptation bubbles present in the sample can be pressed outward by the conical shape. The cone geometry had a diameter of 60 mm and was characterized by a cone angle of $\alpha = 1.012°$. The gap distance between the cone and the plate was 0.031 mm with a liquid volume of 1.01 mL. The measurement was performed in the shear range between 1 and 1000 s^{-1} with 6 data points per decade to determine the dynamic viscosity as a function of the shear rate. Viscosity curves were generated in the upward and downward direction for the triple-produced emulsions per formulation.

2.3.4. Bright field microscopy

Bright-field microscopy was used to investigate the spatial distribution of proteins, lipids and fibers in the prepared liquid samples by being stained with Toluidine blue. The dye stains the proteins in blue, the fibers in magenta, whereas the lipid droplets were identified directly by their characteristic spherical morphology. Toluidine blue (Sigma–Aldrich, The Netherlands) was diluted at 1 mg/mL in deionized water. 1 mL of liquid sample was stained by the addition of a 10 μL drop of Toluidine blue solution. A drop of the stained sample was placed between a microscopy slide and a cover slide and observed with an Axioplan optical microscope (Zeiss, Germany) in bright field mode using 10x, 20x and 40× objectives.

2.3.5. Fluorescence microscopy

Fluorescence microscopy was used to investigate in detail the spatial distribution of proteins, lipids and fibers in the liquid samples by being stained with Fast Green, Nile Red and CalcoFluorWhite, respectively. The analysis was conducted according to Michel et al. (2022). Nile Red (Sigma–Aldrich, The Netherlands) was diluted at 0.25 mg/mL in ethanol (Fisher Scientific, The Netherlands), Fast Green (Sigma–Aldrich, The Netherlands) was diluted at 1 mg/mL in deionized water and CalcoFluorWhite (Sigma–Aldrich, The Netherlands) at 1 mg/mL and Potassium Hydroxide (Fisher Scientific, The Netherlands) at 10%. 1 mL of liquid sample was stained by the addition of a 10 μL drop of Nile Red solution, followed by a 10 μL of Fast Green solution, 10 μL of CalcoFluorWhite solution and 10 μL of KOH solution. A drop of the stained sample was placed between a microscopy slide and a cover slide and observed with a LSM710 upright confocal microscope equipped with Airyscan detector (Zeiss, Germany) using Plan-Apochromat objectives (10x/0.45, 20x/0.8, 63x/1.4). The excitation laser lines used were 405, 488 and 633 nm for CalcoFluorWhite, Nile Red and Fast Green, respectively. Images were acquired and processed with the ZEN imaging software (Zeiss, Germany).

2.3.6. Preparation of dispersions

Prior to interfacial measurements, SPI, OB and SPI-OB mixtures ($3\%_{wt}$) were prepared in MilliQ water adjusted at pH 7 and stirred with a rotor-stator mixer for 20 min. Insoluble compounds were removed by centrifugation at $4000 \times g$ for 20 min. The total solid content (%TS) in the supernatant was measured by thermogravimetric analysis. The dispersions were diluted to $0.1\%_{wt}$ for interfacial analysis.

2.3.7. Drop tensiometer measurements

The interfacial tension between the sunflower oil and the protein solutions as a function of time $\gamma(t)$ was determined with a drop tensiometer (TECLIS Instruments, France). An oil droplet is generated at the tip of the needle and the surface tension was calculated based on the shape of the drop according to the Young-Laplace equation shown in Eq. (1):

$$\Delta p = \gamma \bullet \left(\frac{1}{R_1} + \frac{1}{R_2}\right) \tag{1}$$

The latter relates the pressure difference across the interface Δp and the mean surface curvature knowing the value of both radii $\left(\frac{1}{R_1} + \frac{1}{R_2}\right)$. From the value of the interfacial tension γ, surface pressure can be determined as $\pi_t = \gamma_0 - \gamma_t$ with γ_0 as the value of the initial surface tension. For the experiments, an oil droplet of 30 mm^2 was created at the tip of a rising needle (outer diameter of 1.65 mm). The oil droplet is immersed in a $0.1\%_{wt}$ dispersion. The interfacial tension was continuously monitored for 3600 s at approximately 20 °C. SPI and OB were measured separately as well as 20:1, 10:1, 3:1 SPI-OB mixtures following the emulsions recipes. After 3600 s, the interfacial elastic ($E_D^{'}$) and viscous ($E_D^{''}$) moduli were measured with oscillatory dilatational interfacial rheology (Hinderink et al., 2020). The moduli were characterized as a function of amplitude deformation. The oil droplet was subjected to sinusoidal deformation (cycle of expansion and compression) with an amplitude between 2 and 25% of the original volume at a constant frequency of 0.1 Hz. Each amplitude consisted of a series of 5 deformation cycles followed by 1 cycle of rest period and an equilibrium back to the original volume of 180 s before the next deformation cycle. Based on the phase angle θ, both dilatational elastic modulus ($E_D^{'}$) and dilatational viscous modulus ($E_D^{''}$) can be calculated based on Eqs. (2) and (3) as:

$$E_D^{'} = |E_D| \bullet \cos\theta \tag{2}$$

$$E_D^{''} = |E_D| \bullet \sin\theta \tag{3}$$

The dilatational modulus E_D can be determined by the Gibbs equation. Each experiment was repeated at least three time to ensure repeatability.

2.4. Analysis of particle properties

2.4.1. Particle size measurements

The particle shape and size distribution were analyzed using dynamic image analysis based on the 2-camera principle of the CamSizer XT (Retsch Technology, Germany) (Pietsch et al., 2018). The measurement was performed with compressed air dispersion and a dispersion pressure of 90 kPa. The analysis enabled the particle size distribution and the characteristic parameters to be determined. In addition, the Sauter mean diameter was calculated based on the distribution using the software Matlab. To ensure repeatability, the measurements were repeated at least three times.

2.4.2. Electron microscopy

Electron microscopy was used to investigate the morphology of the powder samples (Munoz-Ibanez et al., 2015) and the spatial distribution of the lipids by being stained with Osmium Tetroxide (OsO_4, EMS,

United States). Therefore, the powder was spread on an aluminum microscopy stub equipped with a conductive carbon sticker. The surface of the stub was gently tapped with a razor blade to open the powder particles and access its interior. The specimens were exposed to OsO_4 vapor for 4 h to stain the unsaturated lipids. The specimens were observed with a Scanning Electron Microscope (SEM) Quattro S (Thermo Fisher, United States) employing the backscattered electron detector, which provides topography contrast and elemental contrast to locate the lipids stained with OsO_4. Imaging was performed at an accelerating voltage of 10 kV and in low vacuum mode to reduce charging artifacts.

2.4.3. Moisture content

For determining the moisture content of the PBMA powder after the spray drying process, the moisture analyzer EM 120-HR (Precisa Gravimetrics AG, Switzerland) was used. The method is based on thermogravimetry at a temperature of 102 °C for 30 min. The measurement was performed with all manufactured powders in triplicates.

2.4.4. Surface lipid analysis

The concentration of lipids on the particle surface was analyzed to assess the encapsulation efficiencies. The surface lipids are the oil proportion which is not encapsulated during the spray drying process. The analysis was conducted following a protocol by Haas et al. (2019) and Sarkar et al. (2016) with modifications. The measurement was performed in triplicates with 2 g of PBMA powder dissolved in 40 mL of n-heptane. To obtain optimal lipid release from the particle surface, the dispersion was stirred at 300 rpm for 10 min in a laboratory shaker. After a sedimentation phase lasting 30 min, the liquid supernatant was separated from the particulate solid. Centrifugation at 2,000 rpm for 5 min led to re-sedimentation of the remaining powder particles. The liquid phase was then aspirated with a syringe and filtered through a sterile filter. A volume of 25 mL of the filtrate was filled onto pre-weighed aluminum pans and the solvent in the pans were evaporated at 115 °C on a heating plate. Once evaporation was complete, heating was continued for an additional 10 min. The aluminum pans were dried for 30 min at 100 °C in a heating oven and cooled in a desiccator with silica gel for at least 1 h. By weighing the pans, the concentration of the oil at the particle surface and the encapsulation efficiency (EE) of the lipid droplets in the particle matrix were determined for the formulations considering the moisture content. For this purpose, the mass differences of the total fat content m_{TF} from the fraction located on the surface m_{SF} was related to the total oil content in Eq. (4):

$$EE = \frac{m_{TF} - m_{SF}}{m_{TF}} \tag{4}$$

2.4.5. Particle density and closed porosity

The apparent solid density was evaluated using the AccuPyc 1330 helium pycnometer (Micromeritics, United States) and corresponded to the volume of the solid phase including the closed pores (Haas et al., 2019). The closed porosity ε_{closed} was also determined with the helium pycnometer (Fuchs et al., 2006) and calculated based on Eq. (5) knowing the sample density without processing ρ_s and after crushing the particles ρ_c:

$$\varepsilon_{closed} = 1 - \frac{\rho_s}{\rho_c} \tag{5}$$

For each powder produced, six individual measurements were conducted.

2.4.6. Statistical evaluation

The results were reported as mean ± standard deviation and the statistical analyses was determined using one-way ANOVA with $\alpha = 0.05$. The Tukey's multiple comparison test was applied in Origin (2021b). Significant differences were indicated in the text and by different letters in the tables when $p < 0.05$ were obtained. The number of trials and measurement repetitions are listed in the corresponding sections.

3. Results and discussion

3.1. Influence of protein and fiber on the emulsion characteristics

3.1.1. Droplet breakup

The emulsion and powder quality of the product are strongly dependent on the homogenization of the PBMA components. In order to control the properties of both product forms, the material influence on the droplet size distribution, which had not previously been described, was first investigated. Homogenization in the high-pressure homogenizer causes a significant reduction of the distribution towards smaller droplet diameters (see Fig. 1). The droplet size decreases with increasing applied homogenizing pressure except of PP1, but the SPAN value is not reduced by the processing step (see Table 2). As the formulation PP1 differs due to the increased concentration of OB, the formation of fiber aggregates during homogenization is possible. The increase in SPI in PP2 results in slightly smaller oil droplets compared to the reference formulation PP3, which also leads to significant differences ($p < 0.05$) in the statistical data analysis. Therefore, it can be assumed that the concentration of the emulsifier at the interface has reached its maximum, and further increments will not lead to any enhancement in emulsion quality. Hu et al. (2003) found protein saturation at the droplet interface even at low concentrations of casein, whey protein isolate and soy protein isolate.

Fig. 2 depicts the microscopic images of the PBMA emulsions after homogenization at 250/50 bar. The oil droplets are isolated in the continuous phase, so the measurement of aggregates formed by oil droplets during the droplet size analysis can be excluded. This observation was found for all formulations and homogenization pressures. The OB components indicated by arrows in the microscopic images exceed the dispersed droplet diameter despite the homogenization step. In the study by Michel et al. (2022) on plant-based cream cheese made from pea protein, sunflower oil and pea/potato fibers, comparable size pattern were noted in the confocal microscopy images. Particularly in Fig. 2 b), network-like structures are visible in the PBMA emulsion, which can be attributed to the oat components and form a steric barrier. In addition to the soluble fiber β-glucan, OB contains proteins that can interact with the interface and improve emulsion stability.

Besides the microscopic analysis, the components used in the formulations were individually examined in order to understand the trimodal droplet size distribution curve of the homogenized PBMA emulsions in detail (see Fig. 3). Therefore, the ingredient OB was dissolved in water, homogenized at 250/50 bar and then measured. Centrifugation enabled the oil droplets to be separated and analyzed from the 250/50 bar homogenized emulsion as a function of the formulation ratios. The OB in the continuous phase is characterized by a bimodal distribution, the comminution of the OB and fiber component thus determines the width of the droplet size distribution in addition to the droplet break-up. Furthermore, the statistical evaluation did not indicate any significant differences ($p < 0.05$) between the oil droplet curves of the plant-based formulations. The results of the particle size analysis thus confirm the size differences of the components identified in the light microscope images. The increased concentration of SPI in PP2 leads to a more pronounced bimodal distribution in Fig. 3. Consequently, protein molecules that are not adsorbed as multilayers at the interface tend to aggregate within the continuous phase. Coalescence processes occurring between the oil droplets during homogenization are also expected. The comparison of the formulations demonstrate that the soy proteins act substantially at the interface. Nishinari et al. (2014) describe greater interactions of the 7S globulin molecules in the SPI and stronger protein film formation on the oil droplets. In the study of Hu et al. (2003), the droplet size of the disperse phase in the O/W emulsion

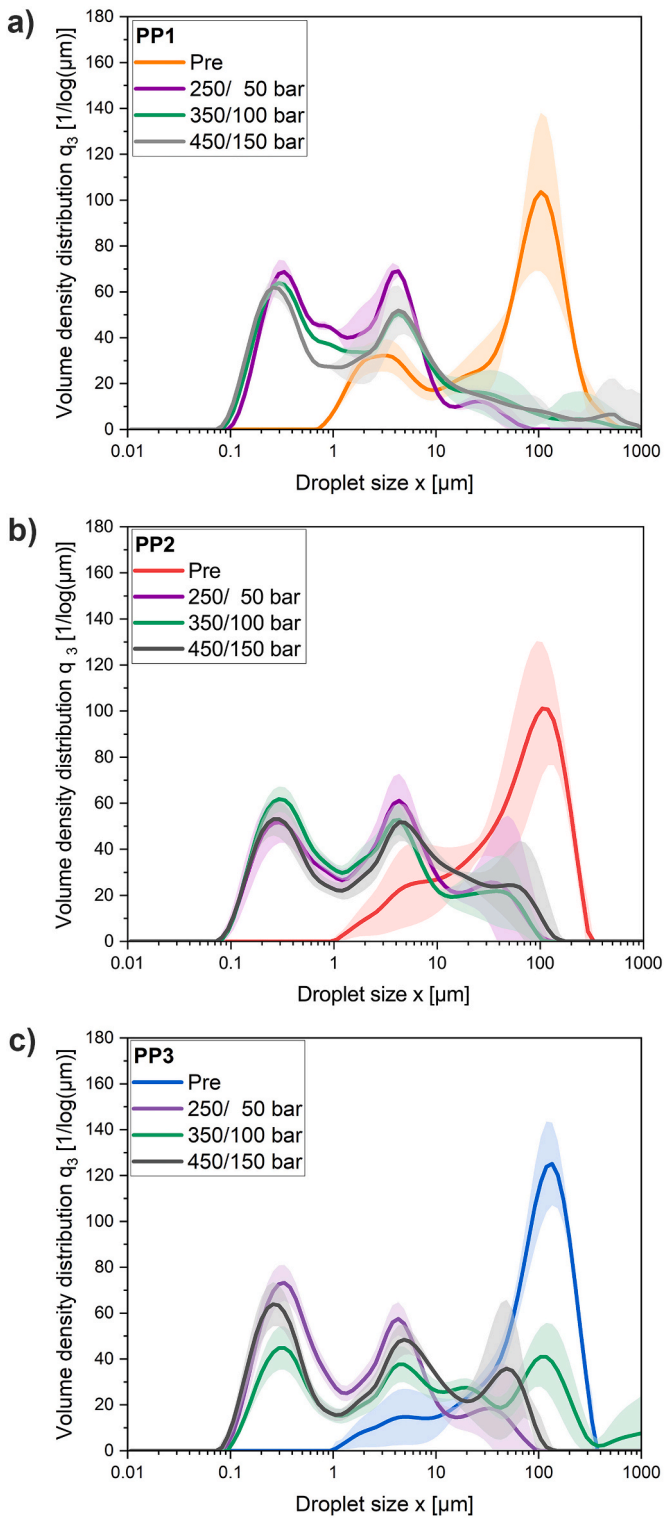

Fig. 1. Volume density distribution of the pre- and homogenized emulsions produced at different homogenization pressures for the formulations a) PP1, b) PP2 and c) PP3.

as well as the droplet charge and accompanying specific emulsifier properties have an effect on lipid oxidation. To regulate oxidation in the PBMA product, the following investigations are focused on the phase interface.

3.1.2. Stabilization of the interface

The proteins acting as emulsifiers in the PBMA emulsions stabilize the oil droplets by inducing an electrical charge that causes repulsive forces between the droplets, thus making the system stable regarding coalescence and flocculation (Hu et al., 2003). Due to the adsorption of the emulsifying components at the interface, steric interactions of various strengths can also occur depending on the formed interfacial layer which prevent destabilizing effects in the product system (Shao et al., 2020). In emulsions with proteins as emulsifier system, the interfacial layers are usually relatively thin, thus electrostatic effects dominate steric repulsion (Zhang et al., 2021). The zeta potential was measured to estimate the emulsion stability, representing the electrical potential in the bilayer at the phase interface (Qi et al., 2021). In Fig. 4, the magnitude of the zeta potential decreases with storage time, indicating that the PBMA emulsions become increasingly instable. The influence of the homogenizing pressure is not significantly different within the formulations ($p < 0.05$). To understand the course in more detail, the pH value was measured, as the charge of the proteins depends on the pH value of the surrounding solution. The homogenization process did not destroy the microorganisms present in the emulsion, and the pH value decreases to acidic levels due to acetate formation during anaerobic metabolism. The increased concentration of oat fiber in PP1 leads to the fastest decrease in pH value and is also reflected in the most instable emulsions on day 4. Otherwise, the highest concentration of SPI in PP2 results in more stable PBMA emulsion systems. Shao et al. (2020) provided evidence that polysaccharides, when not adsorbed at the interface, exert a stabilizing effect on emulsions by reducing destabilization. In the study of O'Flynn et al. (2021), the zeta potential of SPI dispersions was investigated as a function of pH value. A significant decrease in the negative net charge of the zeta potential was observed at pH value < 6.0. Nishinari et al. (2014) and O'Flynn et al. (2021) attribute this observation partly to the change in the tertiary and quaternary structure of β-conglycinin and glycinin, which affect the hydroelectric charge and protein interactions. The potential values measured on day 0 correspond to those reported in literature (O'Flynn et al., 2021), but the differences increase with the storage time. Therefore, the decrease in zeta potential can be ascribed to microbial growth and the associated metabolism, thus influencing the emulsion environment through pH value alterations. The PBMA emulsions consequently approach the isoelectric point of SPI (pI ≈ 4.6 (O'Flynn et al., 2021; Wolf, 1970), leading to a decrease in solubility. Immediately after the homogenization process, the electrical charge induced by the SPI can be assumed to predominate. The analysis of PBMA emulsion stability as a function of formulations and homogenization pressures is intended to provide insights into the storage time at which a consistently stable emulsion can be ensured for further processing steps. The previously not studied correlation of PBMA stability over storage time is thereby also of industrial relevance. Due to the instabilities occurring with increasing storage time, the emulsions were spray-dried immediately after homogenization on day 0 (see section 3.2).

3.1.3. Rheological properties

The not yet identified rheological properties of the PBMA formulations had been investigated to characterize the material influence on the production process and the microstructure of the O/W emulsions. Fig. 5 show shear-thinning flow behavior for the plant-based emulsions. Due to the homogenization process, the flow behavior increasingly approaches a Newtonian fluid. The rheological property described was also observed in the study of Kivelä et al. (2010) using oat β-glucan solutions. For all formulations, high-pressure homogenization leads to a reduction in dynamic viscosity. Among the used homogenization pressures, no significant differences can be identified by the statistical analysis. In the investigations of Pal (1996) an opposite trend is described as a result of high-pressure homogenization. The droplet size has a decisive influence on the emulsion rheology by increasing the viscosity with a higher proportion of fine droplets compared to the pre-emulsion. Furthermore,

Table 2
Characteristic droplet size parameters for the different PBMA formulations and processings in the high-pressure homogenizer at different homogenizing pressures.

Formulation	Pressure [bar]	$x_{10,3}$ [μm]	$x_{50,3}$ [μm]	$x_{90,3}$ [μm]	$x_{3,2}$ [μm]	$x_{4,3}$ [μm]	SPAN [−]
PP1	Pre	2.7 ± 0.4^{a}	60.9 ± 21.2^{a}	181.3 ± 6.0^{a}	10.3 ± 0.7^{b}	78.8 ± 0.6^{b}	2.9 ± 0.7^{a}
	250/50	0.2 ± 0.0^{b}	1.3 ± 0.2^{b}	9.3 ± 8.9^{a}	0.6 ± 0.0^{b}	5.6 ± 0.6^{b}	8.9 ± 2.1^{b}
	350/100	0.2 ± 0.0^{a}	1.5 ± 0.3^{a}	27.1 ± 10.4^{b}	0.6 ± 0.0^{a}	8.6 ± 3.0^{a}	16.9 ± 1.3^{a}
	450/150	0.2 ± 0.0^{a}	2.1 ± 1.1^{a}	44.4 ± 27.9^{a}	0.6 ± 0.0^{a}	31.4 ± 16.7^{a}	21.9 ± 4.7^{a}
PP2	Pre	6.0 ± 2.5^{b}	61.4 ± 16.8^{a}	167.0 ± 5.2^{b}	17.0 ± 3.2^{a}	74.9 ± 1.1^{c}	2.6 ± 0.2^{a}
	250/50	0.3 ± 0.0^{a}	4.8 ± 0.6^{a}	88.7 ± 11.6^{b}	1.0 ± 0.1^{a}	28.2 ± 2.0^{a}	16.0 ± 1.0^{a}
	350/100	0.2 ± 0.0^{a}	2.9 ± 0.2^{a}	45.7 ± 4.9^{b}	0.7 ± 0.0^{a}	14.1 ± 0.6^{a}	15.9 ± 0.8^{a}
	450/150	0.2 ± 0.0^{a}	2.7 ± 0.4^{a}	39.4 ± 4.7^{a}	0.6 ± 0.0^{a}	11.7 ± 1.8^{a}	14.1 ± 1.1^{b}
PP3	Pre	9.2 ± 2.7^{b}	93.3 ± 4.2^{a}	208.0 ± 2.9^{c}	22.4 ± 2.0^{a}	103.0 ± 0.5^{a}	2.1 ± 0.0^{a}
	250/50	0.2 ± 0.0^{b}	4.8 ± 0.5^{a}	101.0 ± 10.2^{c}	$0.8 \pm 0.2^{a,b}$	32.2 ± 3.5^{a}	19.3 ± 2.0^{a}
	350/100	0.2 ± 0.0^{a}	3.0 ± 1.2^{a}	151.0 ± 34.8^{a}	0.6 ± 0.1^{a}	12.6 ± 4.7^{a}	13.5 ± 4.4^{a}
	450/150	0.2 ± 0.0^{a}	2.8 ± 0.6^{a}	43.3 ± 15.8^{a}	0.6 ± 0.0^{a}	11.9 ± 1.5^{a}	$15.2 \pm 2.4^{a,b}$

*values associated with different letters per applied pressure denote significant differences ($p < 0.05$) between the PBMA formulations PP1, PP2 and PP3.

the shear-thinning flow behavior of the fine emulsions is more pronounced as a result of homogenization, which is attributed to the presence of an electrical double layer due to surfactant adsorption at the interface (Pal, 1996). For the investigated PBMA emulsions, the effect of the stabilizing double layer can be considered small since the droplet size exceeds. The addition of SPI to the O/W emulsion results in a significant viscosity increase, necessitating the adjustment of the PP2 formulation in terms of the total solids content during emulsion preparation (see section 2.2.1). An adjustment was inevitable due to pumping and atomization efficiency in the process. Since all formulations are in the same pH value range, differences in protein solubility can be neglected (O'Flynn et al., 2021). O'Flynn et al. (2021) described shear-thinning flow behavior for dispersions containing SPI, but protein aggregates were observed at pH 6.9. The deviations in the range of low shear rates shown in Fig. 5 can probably be attributed to the formation of aggregates as well as sedimentation of the fiber particles. As the shear rate increases, the aggregates break up and sedimentation processes are avoided (González-Tello et al., 2009; Pal, 1996). In the high shear rate regime, the dispersed particles can also align to the shear plane reducing the frictional resistance (Song et al., 2013). Song et al. (2013) conducted investigations on SPI and found a viscosity reduction at all shear rates for the homogenized to the non-treated samples. The alteration of protein structure and viscosity is attributed to the disruption of covalent bonds and inhibition of non-covalent interactions, in addition to the size reduction resulting from high-pressure homogenization (Song et al., 2013). Consequently, the protein influence on the rheological emulsion properties are higher than increasing oil droplet concentration due to the high-pressure homogenization process.

In literature, aqueous solutions containing the fiber β-glucan exhibit non-Newtonian shear-thinning flow behavior (Agbenorhevi et al., 2011; Kivelä et al., 2010; Wood, 2010). Kivelä et al. (2010) showed a linear relationship of viscosity decline with increasing shear rate to the molar mass and thus particle size of the fiber, which decreased with increasing mechanical energy input in the high-pressure homogenizer. The greater the concentration of fiber in the dispersions, the higher is the degree of fragmentation at constant homogenization (Kivelä et al., 2010). According to the study of Agbenorhevi et al. (2011), the shape and size of the formed aggregates increases with higher fiber concentration. Especially in the rheological measurements at low shear rates, hysteresis occurs between the upward and downward viscosity curves, this is depicted by the deviations in Fig. 5 respectively. Agbenorhevi et al. (2011) attributed the behavior to aggregate formation as well as interactions between the fiber particles. Considering the microscopic images (Fig. 6), the oil droplets stained in red can be seen to exist in different sizes in the continuous phase due to coalescence phenomena. Due to the very small molecular size of the proteins, the aggregates stained in green formed multilayers around the disperse phase. However, the size of the fibers stained in blue outweighs the other components, suggesting that the oat fibers are a major influence on the rheological emulsion properties. The statistical data analysis also confirms the suggestion showing a significant influence ($p < 0.05$) of formulation PP1 with increased fiber content. Furthermore, the microstructural characteristics described for the PBMA emulsions align with the studies involving plant proteins (Amagliani et al., 2023; Guldiken et al., 2023; Michel et al., 2022).

3.1.4. Interfacial tension measurement

Adsorption kinetics at oil-water interface and calculated surface pressure over time are presented in Fig. 7. All samples indicate significant differences ($p < 0.05$) in the statistical evaluation. In the diagram, various regimes are visible in adsorption kinetics. An initial and rapid decrease of interfacial tension is linked to the adsorption of surface-active compounds at interface. Then, adsorption slows down and interfacial tension decreases more slowly. This phenomenon is explained by the rearrangement of interfacial compounds, which reorganize themselves to lower the interfacial tension as much as possible (Yang and Sagis, 2021). At oil-water interface, SPI solution led to the highest surface pressure around 13.7 mN/m and OB solution to the lowest (~12.3 mN/m). The curves corresponding to the mixtures of SPI-OB show an intermediate behavior to that of the compounds measured individually. It is important to specify that the measurements were made at a solid content equal to 0.1%. Therefore, the protein content in SPI dispersion is higher than the one in OB dispersion and the overall total content of surface-active compounds in both dispersions might be different. However, it worth notice that OB also contain various compounds which can present specific surface activity such as fibers of small polar lipids. To have a better understanding on the interfacial layers organization, dilatational rheology was performed.

3.1.5. Interfacial dilatational rheology

Oscillatory dilatational amplitude strain sweep (deformation ranging from 2% to 25%) were performed at a frequency of 0.1 Hz after 1h of equilibrium (see Fig. 8). The calculated dilatational elastic modulus was much higher than the viscous modulus for all dispersions indicating a more elastic behavior. Similar results for SPI solution were observed by Zhang et al. (2021). At sunflower oil-water interface, the elastic modulus of OB slightly decreased upon deformation from 11.7 mN/m (at 2% volume deformation) to 10.4 mN/m (at 25% volume deformation). The elastic moduli of SPI and SPI-OB dispersions showed almost no strain dependency. The absence of strain dependence indicated the presence of weak plane-plane interactions at interface (Hinderink et al., 2020). The dispersion 20:1 SPI-OB and 10:1 SPI-OB behave similar as the SPI alone, indicating that only SPI protein adsorbed at interface or that the configuration and interfacial organization is similar for these two mixtures and for the SPI alone. An unexpected behavior is the evolution of the dilatational elastic modulus for the mixture containing 3:1 SPI-OB. The statistical investigations reveal significant differences ($p < 0.05$) between this mixing ratio and the other samples. The dilatational elastic modulus of 3:1 SPI-OB was the lowest for all strain tested ranging from 9.4 (at 2% volume deformation) to 9.2 mN/m (at 25% volume

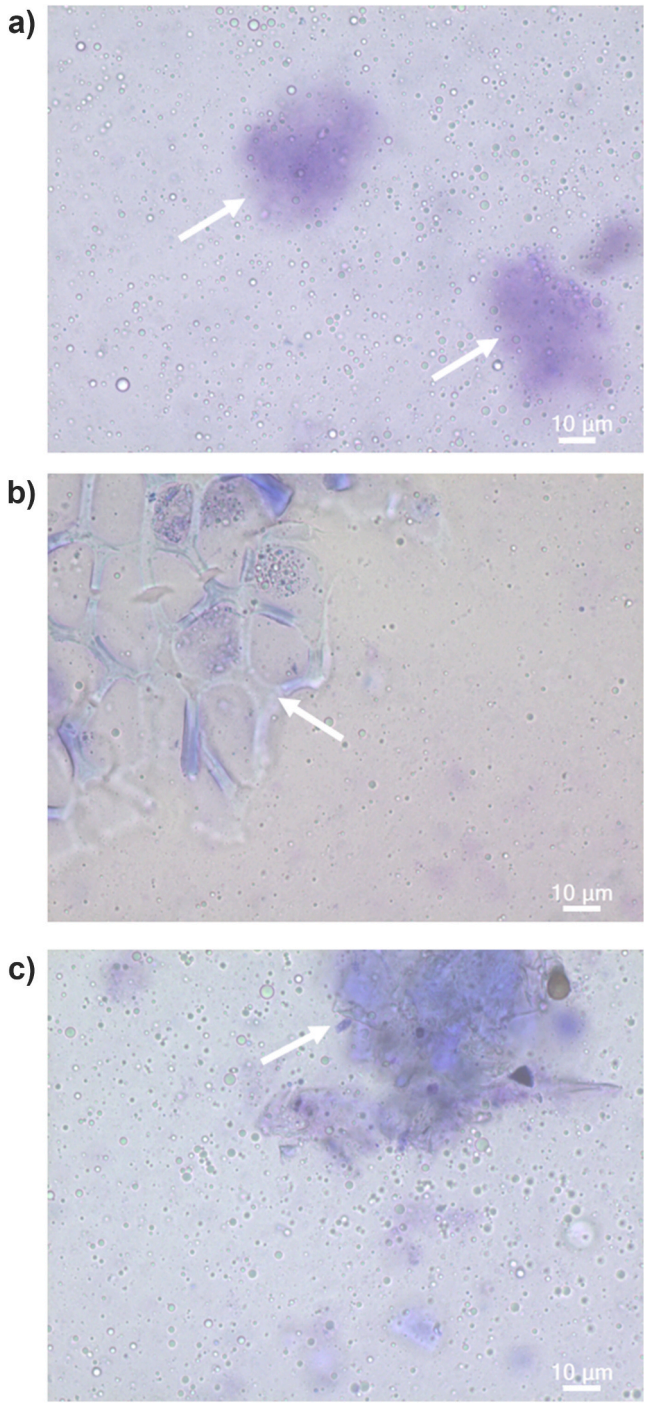

Fig. 2. Light microscope images of the PBMA formulations a) PP1, b) PP2 and c) PP3 homogenized at a pressure of 250/50 bar; the arrows illustrate the oat bran structures in the emulsions, which are significantly larger than the oil droplet diameters; in b) the exposure was adjusted to improve the clarity of the fiber component.

deformation) indicating some very weak interaction at interface and the absence of a strong network. The lower elastic modulus compared to the SPI and OB dispersion alone suggested the presence of both compounds at the interface and the absence of a synergistic effect. An increase in OB concentration seemed to hinder and impact the formation of SPI network at interface. This could be explained by the existence of steric hindrance which will be weaken the formed interface.

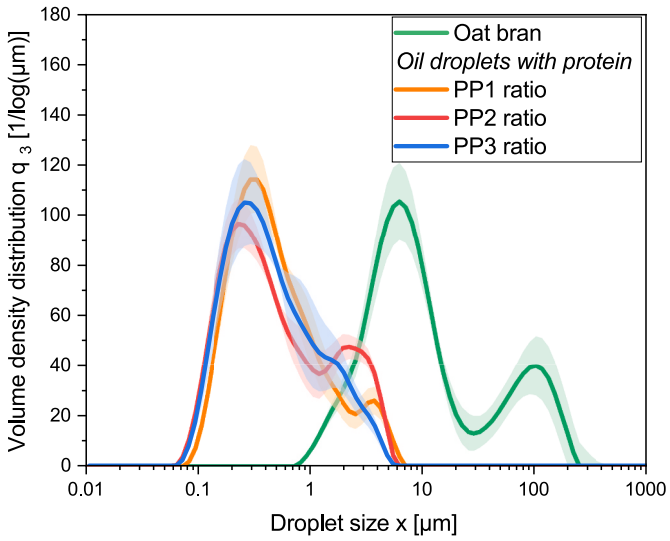

Fig. 3. Volume density distribution of OB solution and the oil droplets stabilized with protein depending on the different PBMA formulations.

3.2. *Influence of protein and fiber on the powder characteristics*

The emulsions were spray-dried and the resulting particles were analyzed to identify the influence of the PBMA formulation on the powder properties. The increased amount of SPI in PP2 results in the smallest particle diameters, whereas a higher concentration of OB in PP1 leads to an increase in particle size (see Fig. 9, $p < 0.05$). In the emulsion characterization, the fragmentation of the OB and fiber has been demonstrated to have a significant impact on the viscosity. Since the drying parameters were kept constant between formulations, larger droplets are expected at the outlet of the two-fluid nozzle of PP1 and the smallest diameters for PP2. Consequently, the drying rate of the emulsion droplet differs between the different formulations and is characterized in higher moisture contents due to the addition of OB as can be seen in Table 3. As OB is composed of soluble and insoluble fiber material (Gualberto et al., 1997; Manthey et al., 1999), an influence of both fractions on the spray drying process can be expected. The characteristic parameters of particle size distribution, lipid encapsulation, closed porosity and true density are also listed in the table. Boukouvalas et al. (2006) indicates that the true density of food is strongly dependent on the temperature and moisture content of the measured sample. Thus, a direct conclusion on the material characteristics is only possible to a limited extent, since the powders are in different physical states. Furthermore, the particle properties are strongly dependent on the production scale of the spray dryer.

Due to the different component concentration in the PBMA formulations, the surface composition of the solid particles varies by enriching the ingredient used in increased quantities. In the study of Murrieta-Pazos et al. (2012), the surface composition has an influence on lipid accumulation, but in the investigations of Haas et al. (2019) the surface to volume ratio emerges as a crucial parameter of EE. For the spray-dried encapsulated carotenoids, low ratios correlate with high EE (Haas et al., 2019). However, this trend is not observed for the produced PBMA powders in the study. The material influence and the associated particle morphologies significantly affect the surface lipid content. The increased addition of proteins results in a structure characterized by numerous closed pores that contain gas inclusions and lipids (see Table 3 and Fig. 11 a)). According to previous studies (Abdalla and Roozen, 1999), the oxidative stability of PP2 is reported to be higher compared to other formulations as the lowest proportion of oxidation-sensitive sunflower oil is present on the particle surface. In contrast, the fiber component β-glucan leads to less porous particles and the amount of lipids that attach to the surface is higher considering the moisture and

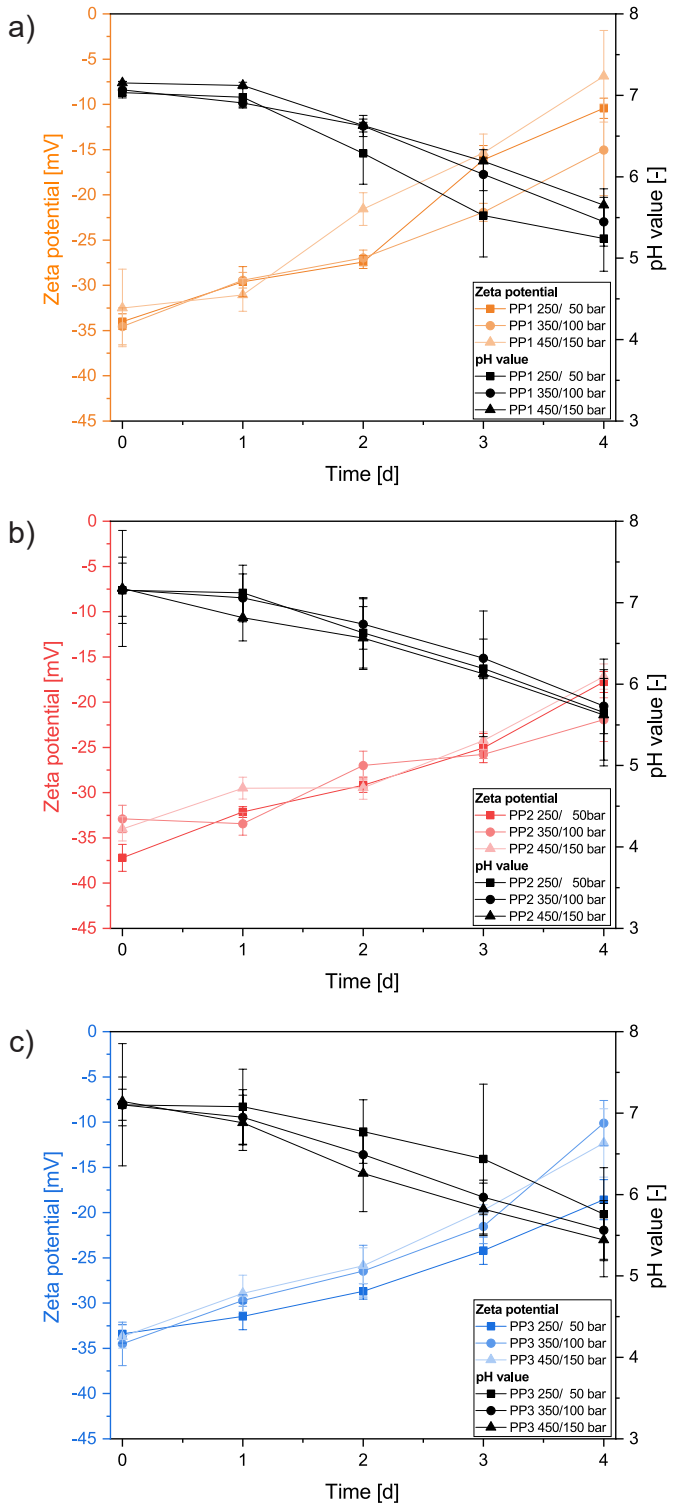

Fig. 4. Zeta potential and pH value as a function of storage time for the O/W emulsions of formulations a) PP1, b) PP2 and c) PP3 produced at different homogenization pressure; the individual measurement points were linked by lines for enhanced readability, the lines do not represent measurements.

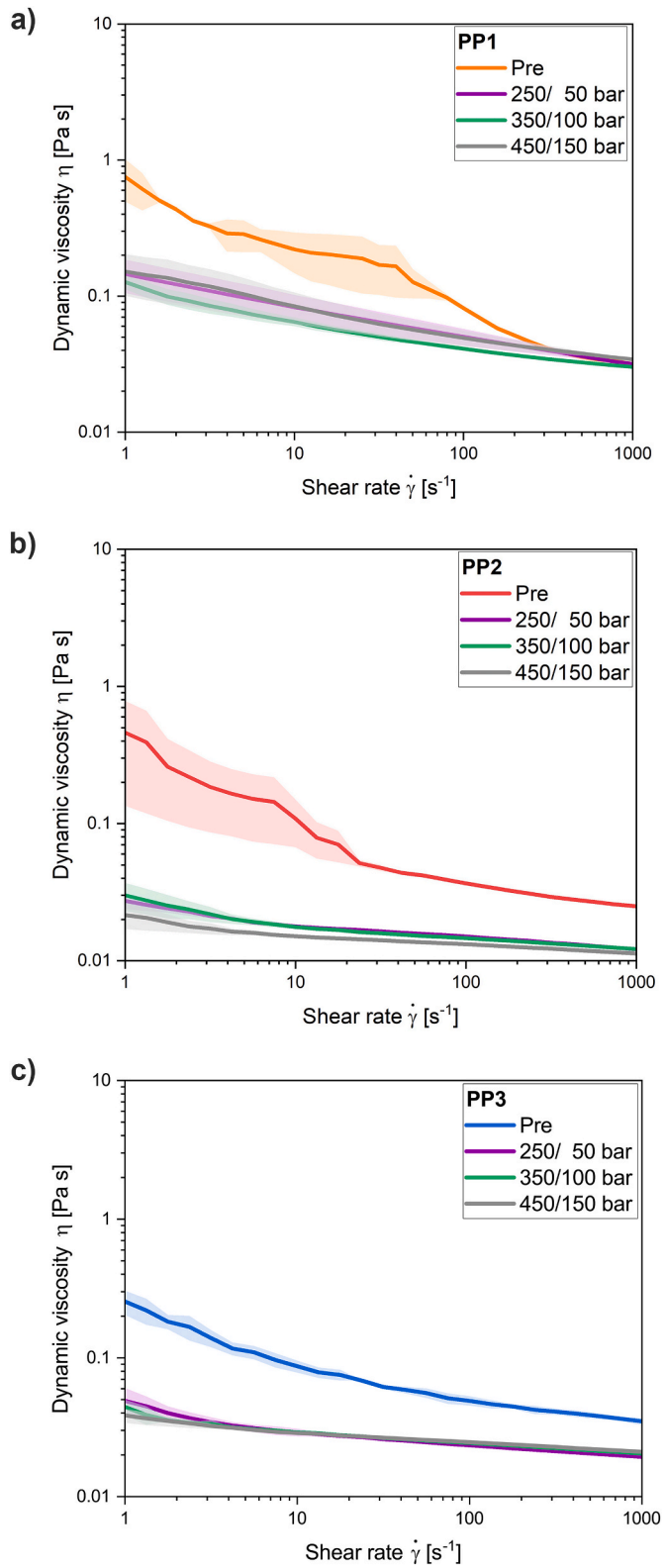

Fig. 5. Dynamic viscosity as a function of shear rate for the pre-emulsion and with different homogenization pressures produced O/W emulsion of formulations a) PP1, b) PP2 and c) PP3.

total lipid content of the formulation. Thus, a lower oxidation stability is to be expected during storage of the powder product. Figs. 10 and 11 confirm the EE results by using the so far unpublished visualization method of the lipid component under the SEM. The figures show that the PBMA formulations are partially agglomerated. The lipid accumulates at the junction of the primary particles, and the formation of agglomerates through lipid bridges cannot be excluded. These particle linkages occurring after the spray drying process have already been described in the literature (Fuchs et al., 2006; Kim et al., 2002). In the investigations of Bhandari (2013), the more wrinkled particle surface is attributed to

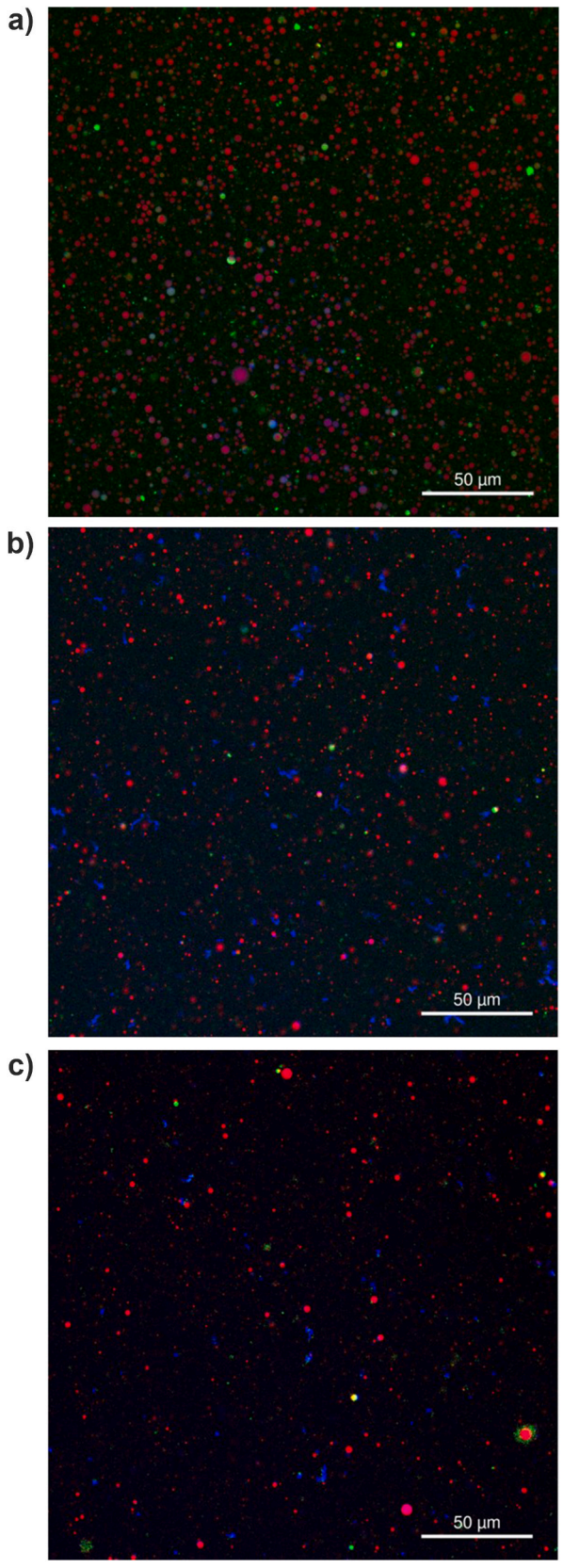

Fig. 6. Fluorescence microscope images to visualize the oil droplets (red), proteins (green) and fibers (blue) in the O/W emulsion of formulations a) PP1, b) PP2 and c) PP3.

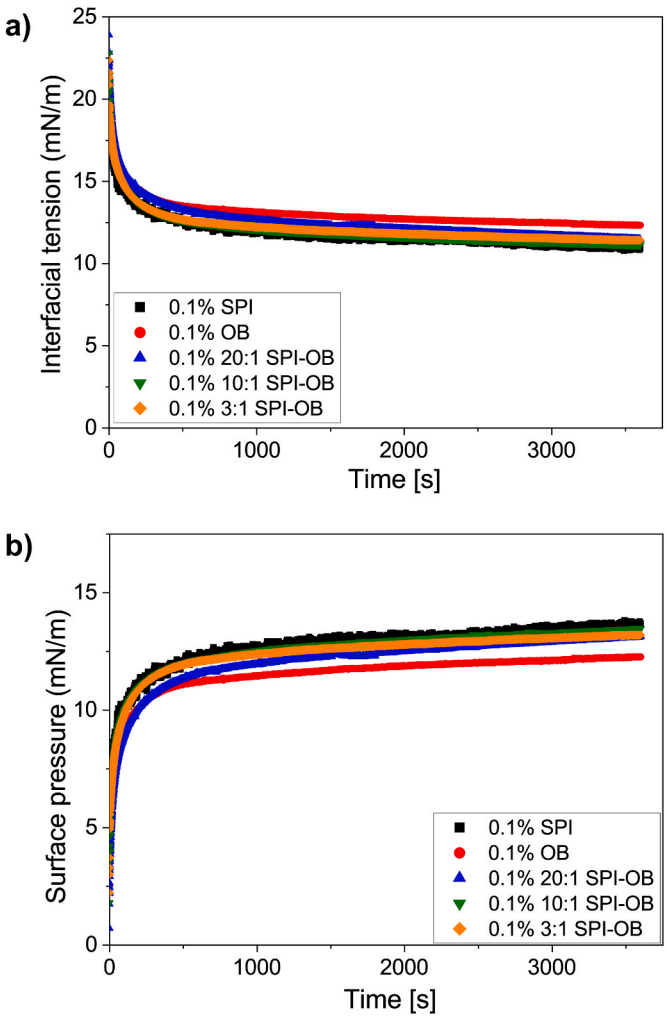

Fig. 7. a) Interfacial tension evaluation over 1h of sunflower oil-water interfaces containing either SPI, OB and different SPI-OB ratios; b) calculated surface pressure over 1h for SPI, OB and different SPI-OB ratios.

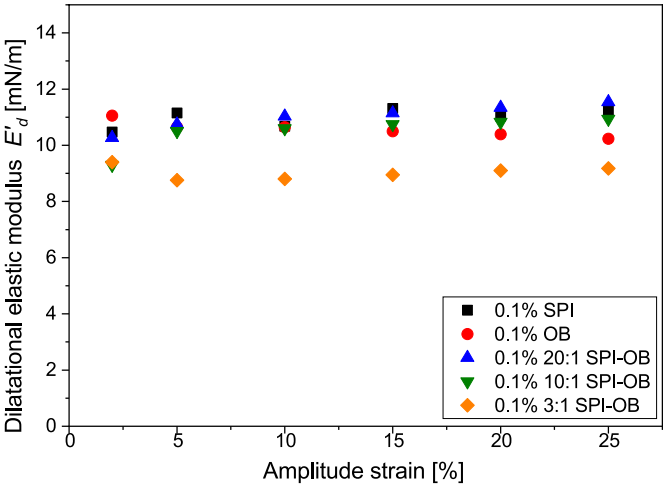

Fig. 8. Dilatational elastic moduli of sunflower oil-water interface stabilized by SPI, OB or SPI-OB mixture as a function of applied deformation and at a fixed frequency (0.1 Hz).

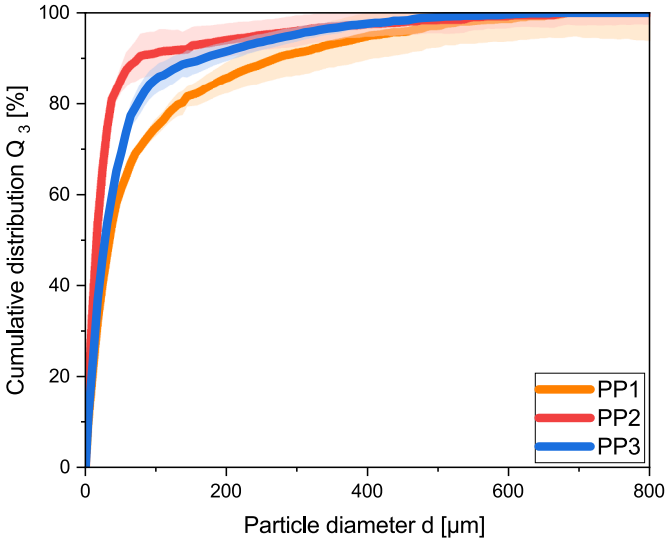

Fig. 9. Particle size distribution of formulations PP1, PP2 and PP3 produced in the spray dryer at constant process parameters.

Table 3
Overview of the characteristic particle properties of the PBMA formulations PP1, PP2 and PP3.

	PP1	PP2	PP3
$d_{10,3}$ [µm]	7.7 ± 1.3^{a}	5.8 ± 0.8^{a}	7.1 ± 0.8^{a}
$d_{50,3}$ [µm]	37.4 ± 4.7^{a}	19.5 ± 2.9^{b}	30.9 ± 1.9^{a}
$d_{90,3}$ [µm]	272.1 ± 56.9^{a}	77.1 ± 23.1^{b}	171.5 ± 20.6^{c}
$d_{3,2}$ [µm]	17.0 ± 3.8^{a}	11.0 ± 2.1^{a}	14.9 ± 1.8^{a}
S [−]	0.80 ± 0.01^{a}	0.81 ± 0.00^{a}	0.81 ± 0.02^{a}
SPAN [−]	7.06 ± 0.57^{a}	3.66 ± 1.20^{b}	$5.31 \pm 0.32^{a,b}$
M_{wb} [g/100 g]	4.17 ± 0.43^{a}	$2.90 \pm 0.38^{a,b}$	3.45 ± 0.50^{b}
ρ_s [kg/m^3]	1240.40 ± 3.78^{a}	1009.25 ± 2.50^{b}	876.45 ± 2.05^{c}
Surface lipid content [%]	3.74 ± 0.19^{a}	1.93 ± 0.18^{b}	$2.16 \pm 0.18^{a,b}$
EE [%]	96.26 ± 0.19^{b}	98.07 ± 0.18^{a}	$97.84 \pm 0.18^{a,b}$
ε_{closed} [%]	3.26 ± 0.69^{c}	7.97 ± 0.45^{a}	4.61 ± 0.37^{b}

*values associated with different letters per row of the characteristic particle property denote significant differences ($p < 0.05$) between the PBMA formulations PP1, PP2 and PP3.

high protein coverage but according to Murrieta-Pazos et al. (2012) the particle morphology is also influenced by drying temperatures and droplet diameter in the spray dryer. Kim et al. (2002) attributed the accumulation of proteins at the particle surface to the enhanced adsorption of proteins at the air/liquid interface during the atomization process in the nozzle and the preferential entrapment of lipids in the matrix. The correlations between the ingredients used in the formulations and the particle properties identified in the section enable targeted product regulation and control of important characteristics such as encapsulation efficiency.

4. Conclusion

The previously unexplored combination of soy protein isolate with oat bran in the complex composition with sunflower oil and glucose syrup DE 21 in the PBMA formulations and their influence on emulsion and powder properties were further investigated. During high-pressure homogenization, the droplet break-up and the width of the droplet size distribution were characterized by the comminution of the fiber component. Furthermore, an improved stabilization of the O/W interface was shown due to an increased fiber concentration and the component significantly influenced the rheological properties of the

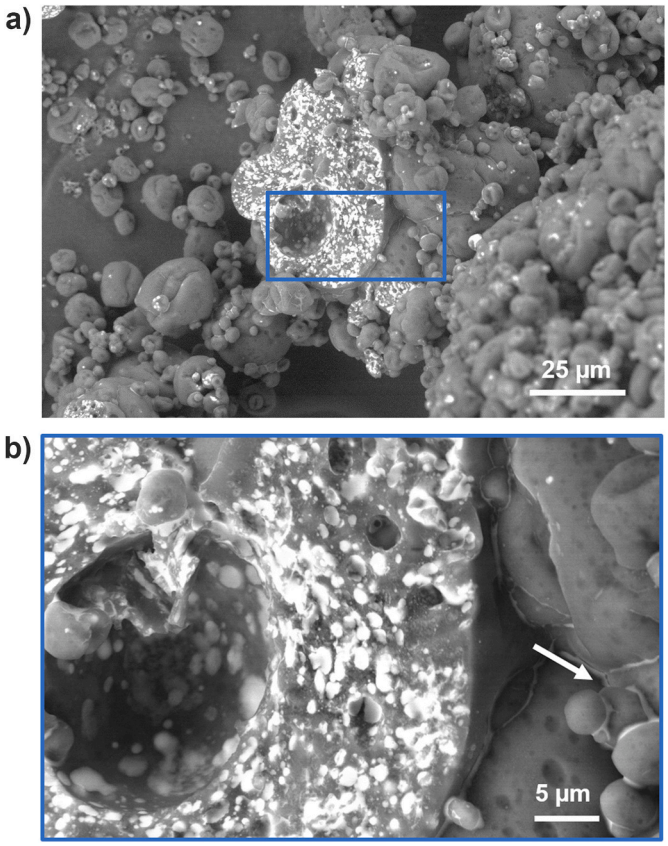

Fig. 10. Electron microscopic image visualizing the lipid component (white) of the spray-dried PBMA formulation PP1 a) at a magnification of 2.5kx and b) at 10kx, the arrow illustrates the lipid accumulations at the junction of the primary particles.

plant emulsions. The investigations at the interface demonstrated that soy protein isolate led to the highest and oat bran solutions to the lowest surface pressures. Deformation also occurred at the interface using oat bran, whereas soy protein isolate and mixtures of the ingredients exerted only weak plane-plane interactions.

The spray-dried milk alternative powder was influenced by the emulsion properties, particularly the dynamic viscosity and fragmentation of the oat bran and fiber. The different component concentrations in the plant-based formulations had an influence on the surface lipid content in addition to the different particle morphologies. The increased addition of the plant proteins in PP2 resulted in a particle structure with many closed pores, which also contained lipids besides to gas inclusions. PP1 with the highest concentration of the fiber β-glucan led to less porous particles and a higher proportion of accumulated lipids on the particle surface. The plant-based milk alternative formulations were partially agglomerated with lipid accumulations at the junction of the primary particles. In order to optimize the reconstitution properties of the increasing industrially relevant milk alternative product and minimize lipid oxidation during storage, it is necessary to identify the most ideal particle morphology in further investigations, additionally to the material influence on the powder structure.

CRediT authorship contribution statement

K. Kramm: Writing – review & editing, Writing – original draft, Project administration, Methodology, Investigation, Conceptualization. **A. Roucher:** Writing – review & editing, Writing – original draft, Investigation, Conceptualization. **J. Busom Descarrega:** Writing – review & editing, Writing – original draft, Investigation. **M. Ambühl:** Investigation. **J. Kammerhofer:** Writing – review & editing,

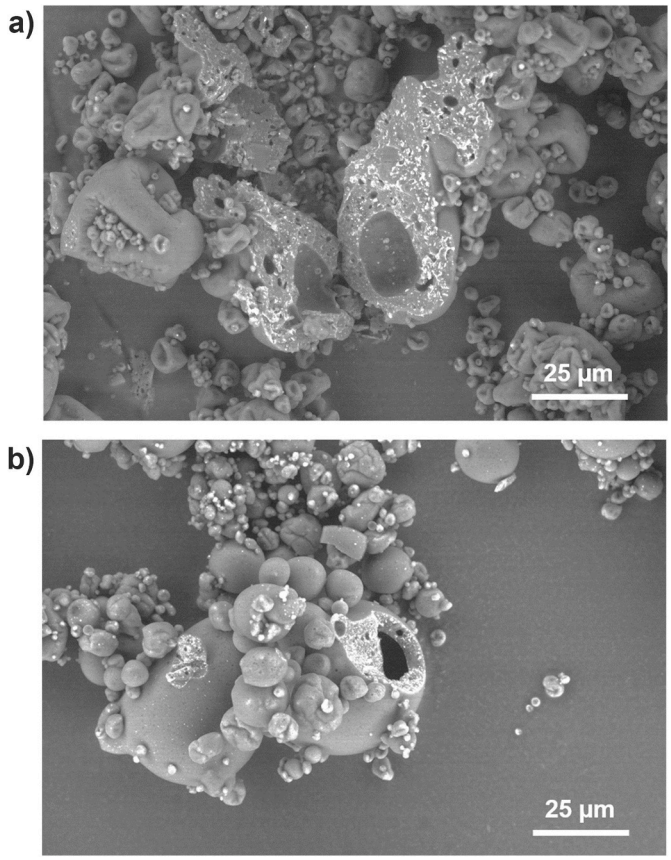

Fig. 11. Electron microscopic image visualizing the lipid component (white) of the PBMA formulation a) PP2 and b) PP3 produced in the spray dryer at a magnification of 2.5kx.

Supervision. **V. Meunier:** Writing – review & editing, Supervision, Funding acquisition. **S. Heinrich:** Writing – review & editing, Supervision, Project administration, Funding acquisition.

Declaration of competing interest

The authors declare that they have no known competing financial interests or personal relationships that could have appeared to influence the work reported in this paper.

Data availability

Data will be made available on request.

Acknowledgment

The author would like to thank Celina Nahrgang for her support with the measurements.

References

Abdalla, A.E., Roozen, J.P., 1999. Effect of plant extracts on the oxidative stability of sunflower oil and emulsion. Food Chem. 64 (3), 323–329. https://doi.org/10.1016/S0308-8146(98)00112-5.

Agbenorhevi, J.K., Kontogiorgos, V., Kirby, A.R., Morris, V.J., Tosh, S.M., 2011. Rheological and microstructural investigation of oat β-glucan isolates varying in molecular weight. Int. J. Biol. Macromol. 49 (3), 369–377. https://doi.org/10.1016/j.ijbiomac.2011.05.014.

Amagliani, L., van de Langerijt, T.M., Morgenegg, C., Bovetto, L., Schmitt, C., 2023. Influence of charged and non-charged co-solutes on the heat-induced aggregation of soy and pea proteins at pH 7.0. Food Hydrocoll. 137, 108392 https://doi.org/10.1016/j.foodhyd.2022.108392.

Armbruster, H., Karbstein, H., Schubert, H., 1991. Herstellung von Emulsionen unter Berücksichtigung der Grenzflächenbesetzungskinetik des Emulgators. Chem. Ing. Tech. 63 (3), 266–267. https://doi.org/10.1002/cite.330630323.

Aydar, E.F., Tutuncu, S., Ozcelik, B., 2020. Plant-based milk substitutes: bioactive compounds, conventional and novel processes, bioavailability studies, and health effects. J. Funct. Foods 70, 103975. https://doi.org/10.1016/j.jff.2020.103975.

Bhandari, B. (Ed.), 2013. *Handbook of Food Powders: Processes and Properties*. Camb. Woodhead Publishing Series in Food Science, Technology and Nutrition, vol. 255. Woodhead. https://doi.org/10.1533/9780857098672.

Boukouvalas, C.J., Krokida, M.K., Maroulis, Z.B., Marinos-Kouris, D., 2006. Effect of material moisture content and temperature on the true density of foods. Int. J. Food Prop. 9 (1), 109–125. https://doi.org/10.1080/10942910500473970.

D'Adamo, C.R., Sahin, A., 2014. Soy foods and supplementation: a review of commonly perceived health benefits and risks. Alternative Ther. Health Med. 20 (Suppl. 1), 39–51. PMID: 24473985.

Fuchs, M., Turchiuli, C., Bohin, M., Cuvelier, M.E., Ordonnaud, C., Peyrat-Maillard, M.N., Dumoulin, E., 2006. Encapsulation of oil in powder using spray drying and fluidised bed agglomeration. J. Food Eng. 75 (1), 27–35. https://doi.org/10.1016/j.jfoodeng.2005.03.047.

Gianfrancesco, A., Turchiuli, C., Dumoulin, E., 2008. Powder agglomeration during the spray-drying process: measurements of air properties. Dairy Sci. Technol. 88 (1), 53–64. https://doi.org/10.1051/dst:2007008.

González-Tello, P., Camacho, F., Guadix, E.M., Luzón, G., González, P.A., 2009. Density, viscosity and surface tension of whey protein concentrate solutions. J. Food Process. Eng. 32 (2), 235–247. https://doi.org/10.1111/j.1745-4530.2007.00213.x.

Gualberto, D.G., Bergman, C.J., Kazemzadeh, M., Weber, C.W., 1997. Effect of extrusion processing on the soluble and insoluble fiber, and phytic acid contents of cereal brans. Plant Food Hum. Nutr. 51 (3), 187–198. https://doi.org/10.1023/a:1007941032726.

Guldiken, B., Saffon, M., Nickerson, M.T., Ghosh, S., 2023. Improving physical stability of pea protein-based emulsions near the isoelectric point via polysaccharide complexation. Food Hydrocoll. 145, 109029 https://doi.org/10.1016/j.foodhyd.2023.109029.

Haas, K., Obernberger, J., Zehetner, E., Kiesslich, A., Volkert, M., Jaeger, H., 2019. Impact of powder particle structure on the oxidation stability and color of encapsulated crystalline and emulsified carotenoids in carrot concentrate powders. J. Food Eng. 263, 398–408. https://doi.org/10.1016/j.jfoodeng.2019.07.025.

Hinderink, E.B.A., Sagis, L., Schroën, K., Berton-Carabin, C.C., 2020. Behavior of plant-dairy protein blends at air-water and oil-water interfaces. Colloids Surf., B 192. https://doi.org/10.1016/j.colsurfb.2020.111015.

Hu, M., McClements, D.J., Decker, E.A., 2003. Lipid oxidation in corn oil-in-water emulsions stabilized by casein, whey protein isolate, and soy protein isolate. J. Agric. Food Chem. 51 (6), 1696–1700. https://doi.org/10.1021/jf020952j.

Kim, E.H.-J., Chen, X., Pearce, D., 2002. Surface characterization of four industrial spray-dried dairy powders in relation to chemical composition, structure and wetting property. Colloids Surf., B 26 (3), 197–212. https://doi.org/10.1016/S0927-7765(01)00334-4.

Kivelä, R., Pitkänen, L., Laine, P., Aseyev, V., Sontag-Strohm, T., 2010. Influence of homogenisation on the solution properties of oat β-glucan. Food Hydrocoll. 24 (6–7), 611–618. https://doi.org/10.1016/j.foodhyd.2010.02.008.

Köhler, K., 2010. *Simultanes Emulgieren und Mischen* (Dissertation). Karlsr. Inst. Technol. (KIT), Karlsruhe. https://doi.org/10.5445/IR/1000021086.

Leal-Calderon, F., Schmitt, V., Bibette, J., 2007. Emulsion Science: Basic Principles. Springer Science+Business Media, New York, NY, p. 2. https://doi.org/10.1007/978-0-387-39683-5. Retrieved from. http://www.loc.gov/catdir/enhancements/fy0818/2007921974-d.html.

Michel, S.E., Scheermeijer, R., Ambühl, M., Fernández Farrés, I., 2022. Novel plant-based cream cheese: a tribology perspective. J. Food Eng. 335, 111172 https://doi.org/10.1016/j.jfoodeng.2022.111172.

Manthey, F.A., Hareland, G.A., Huseby, D.J., 1999. Soluble and insoluble dietary fiber content and composition in oat. Cereal Chem. 76 (3), 417–420. https://doi.org/10.1094/CCHEM.1999.76.3.417.

Mie, G., 1908. Beiträge zur Optik trüber Medien, speziell kolloidaler Metallösungen. Ann. Phys. 330 (3), 377–445. https://doi.org/10.1002/andp.19083300302.

Munoz-Ibanez, M., Azagoh, C., Dubey, B.N., Dumoulin, E., Turchiuli, C., 2015. Changes in oil-in-water emulsion size distribution during the atomization step in spray-drying encapsulation. J. Food Eng. 167, 122–132. https://doi.org/10.1016/j.jfoodeng.2015.02.008.

Murrieta-Pazos, I., Gaiani, C., Galet, L., Scher, J., 2012. Composition gradient from surface to core in dairy powders: agglomeration effect. Food Hydrocoll. 26 (1), 149–158. https://doi.org/10.1016/j.foodhyd.2011.05.003.

Nishinari, K., Fang, Y., Guo, S., Phillips, G.O., 2014. Soy proteins: a review on composition, aggregation and emulsification. Food Hydrocoll. 39, 301–318. https://doi.org/10.1016/j.foodhyd.2014.01.013.

O'Flynn, T.D., Hogan, S.A., Daly, D.F.M., O Mahony, J.A., McCarthy, N.A., 2021. Rheological and solubility properties of soy protein isolate. Molecules 26 (10). https://doi.org/10.3390/molecules26103015.

Pal, R., 1996. Effect of droplet size on the rheology of emulsions. AIChE J. 42 (11), 3181–3190. https://doi.org/10.1002/aic.690421119.

Palzer, S., 2007. Agglomeration of dehydrated consumer foods. In: Salman, A.D., Hounslow, M.J., Seville, J. (Eds.), Handbook of Powder Technology : Granulation, vol. 11. Elsevier Science B.V, pp. 591–671. https://doi.org/10.1016/S0167-3785(07)80048-0.

Palzer, S., 2009. Influence of material properties on the agglomeration of water-soluble amorphous particles. Powder Technol. 189 (2), 318–326. https://doi.org/10.1016/j.powtec.2008.04.034.

Palzer, S., Dubois, C., Gianfrancesco, A., 2012. Generation of product structures during drying of food products. Dry. Technol. 30 (1), 97–105. https://doi.org/10.1080/07373937.2011.622060.

Pietsch, S., Kieckhefen, P., Müller, M., Schönherr, M., Kleine Jäger, F., Heinrich, S., 2018. Novel production method of tracer particles for residence time measurements in gas-solid processes. Powder Technol. 338, 1–6. https://doi.org/10.1016/j.powtec.2018.06.040.

Qi, J., Song, L., Zeng, W., Liao, J., 2021. Citrus fiber for the stabilization of O/W emulsion through combination of Pickering effect and fiber-based network. Food Chem. 343, 128523 https://doi.org/10.1016/j.foodchem.2020.128523.

Romulo, A., 2022. Food processing technologies aspects on plant-based milk manufacturing: review. IOP Conf. Ser. Earth Environ. Sci. 1059 (1), 12064 https://doi.org/10.1088/1755-1315/1059/1/012064.

Sarkar, A., Arfsten, J., Golay, P.-A., Acquistapace, S., Heinrich, E., 2016. Microstructure and long-term stability of spray dried emulsions with ultra-high oil content. Food Hydrocoll. 52, 857–867. https://doi.org/10.1016/j.foodhyd.2015.09.003.

Shao, P., Feng, J., Sun, P., Xiang, N., Lu, B., Qiu, D., 2020. Recent advances in improving stability of food emulsion by plant polysaccharides. Food Res. Int. 137, 109376 https://doi.org/10.1016/j.foodres.2020.109376.

Song, X., Zhou, C., Fu, F., Chen, Z., Wu, Q., 2013. Effect of high-pressure homogenization on particle size and film properties of soy protein isolate. Ind. Crops Prod. 43, 538–544. https://doi.org/10.1016/j.indcrop.2012.08.005.

Statista, 2023. Prognose des Umsatzes mit pflanzlichen Milchprodukten und Milchalternativen weltweit in den Jahren 2019 bis 2029. Retrieved from. https://de.statista.com/statistik/daten/studie/1034861/umfrage/umsatz-mit-alternativen-milchprodukten-weltweit/.

Wolf, W.J., 1970. Soybean proteins. Their functional, chemical, and physical properties. J. Agric. Food Chem. 18 (6), 969–976. https://doi.org/10.1021/jf60172a025.

Wood, P.J., 2010. Oat and rye β-glucan: properties and function. Cereal Chem. 87 (4), 315–330. https://doi.org/10.1094/CCHEM-87-4-0315.

Yadav, D.N., Bansal, S., Jaiswal, A., Singh, Ranjeet, 2017. Plant based dairy analogues: an emerging food. Agric. Res. Technol. Open Access J. 10 (2) https://doi.org/10.19080/ARTOAJ.2017.10.555781.

Yang, J., Sagis, L.M., 2021. Interfacial behavior of plant proteins — novel sources and extraction methods. Curr. Opin. Colloid Interface Sci. 56, 101499 https://doi.org/10.1016/j.cocis.2021.101499.

Zhang, M., Liang, Y., Pei, Y., Gao, W., Zhang, Z., 2009. Effect of process on physicochemical properties of oat bran soluble dietary fiber. J. Food Sci. 74 (8), C628–C636. https://doi.org/10.1111/j.1750-3841.2009.01324.x.

Zhang, X., Zhang, S., Xie, F., Han, L., Li, L., Jiang, L., Li, Y., 2021. Soy/whey protein isolates: interfacial properties and effects on the stability of oil-in-water emulsions. J. Sci. Food Agric. 101 (1), 262–271. https://doi.org/10.1002/jsfa.10638.